IEEE Access
Multidisciplinary | Rapid Review | Open Access Journal

Received 10 August 2024, accepted 22 September 2024, date of publication 30 September 2024,
date of current version 11 October 2024.

Digital Object Identifier 10.1109/ACCESS.2024.3469950

RESEARCH ARTICLE

Novel Peak-Source-Scanning (NPSS) Model for Thermal Control of Systems-in-Package (SiP)

AZIZ OUKAIRA[1], (Member, IEEE), DHAOU SAID[2], (Member, IEEE), DJALLEL EDDINE TOUATI[3], (Member, IEEE), NADER EL-ZARIF[4], (Member, IEEE), AHMAD HASSAN[4], (Senior Member, IEEE), YVON SAVARIA[4], (Life Fellow, IEEE), AND AHMED LAKHSSASSI[3], (Senior Member, IEEE)

[1]Electrical Engineering Department, Université de Moncton, Moncton, NB E1A 3E9, Canada
[2]Department of Electrical and Computer Engineering, Université de Sherbrooke, Sherbrooke, QC J1K 2R1, Canada
[3]Department of Engineering and Computer Science, Université du Québec en Outaouais, Gatineau, QC J9A 1L8, Canada
[4]Electrical Engineering Department, Polytechnique Montréal, Montreal, QC H3T 1J4, Canada

Corresponding author: Aziz Oukaira (aziz.oukaira@umoncton.ca)

ABSTRACT One of the fast-growing electronic integration technologies in the modern high-density microelectronics industry is System-in-Package (SiP). It is expected to accelerate application development when reducing implementation risks with optimized codes. However, monitoring the thermal behavior of every chip in SiPs is challenging. This paper proposes a Novel Peak Source-Scanning (NPSS) algorithm based on the Gradient Direction Sensors (GDS) method. The proposed algorithm can detect and locate thermal peaks on any SiP. Detecting such peaks is vital for thermal monitoring and stress management on high-density semiconductor devices to avoid induced thermo-mechanical stresses. Furthermore, the NPSS algorithm can manage and monitor silicon chips with Multiple Heat Sources (MHS). To assess this algorithm, we used tools from COMSOL Multiphysics® and MATLAB® for Temperature-prediction (Tp), and Temperature-estimation (Te), respectively. Our simulations use the generalized GDS methodology for MHS using the finite element method (FEM) to highlight our NPSS capabilities to predict on-chip thermal peaks with a maximum error of 1.27 K (Kelvin).

INDEX TERMS Peak source-scanning, system-in-package, thermal control, thermal monitoring, thermal peak, finite element method, gradient direction sensors, and multiple heat sources.

I. INTRODUCTION

The Systems-in-Package (SiP) is challenging researchers and industries in integrated circuit (IC) technologies [1], [2], [3], [4]. SiP is mainly based on assembling multiple dies or ICs in single-package dense systems. It also embeds multiple ICs, which can be implemented in different technology nodes for cost-effectiveness. The main objective of SiP is to implement systems that address all the requirements of a functional system without unduly compromising the performance of individual circuits. SiP can extend the system integration beyond the capability of today's mass production process, i.e, surface mount assembly [5]. This evolution towards higher levels of integration is driven by the need for advanced high-performance systems that are lighter, more compact, and consume less power. At the same time, to reduce the overall power consumption, many low-power techniques are used, such as dynamic power management [6], [7]. However, these techniques can generate significant on-chip thermal gradients and local hot spots due to the different clock/power gating activities and variable voltage scaling. Thus temperature gradients of 30 °C could occur on-chip [8]. Nevertheless, the dissipated power density growth leads to several critical thermo-mechanical problems. For example, the heat generated in an IC can be dissipated by radiation, conduction, or convection to reach its edges. Thus, with the lack of efficient dynamic thermal management and added to the direct impact on its life cycle, the IC's performance will continuously decrease, leading to its dysfunction and lockdown [9], [10], [11], [12].

The associate editor coordinating the review of this manuscript and approving it for publication was Wenxin Liu.

In the microelectronics literature, the problem of thermal control and management is well known. Unlike the Systems-on-Chip (SoC) case, where efficient models were proposed to reduce the negative impact of self-heating on circuit operation, there is no practical solution proposed yet for SiPs [13]. Moreover, heat removal is one of the biggest challenges facing SiP designers [14]. Reference [15] presents several techniques used for the thermal management of electronic devices. All these techniques focus on developing solutions suitable for steady-state operations. Moreover, the paper [16] argues that SoCs are increasingly used in applications involving time-varying workloads, partly thanks to proposed and detailed thermal management solutions that can be used to ensure their performance and reliability.

On the other hand, for a better performance of SiPs, the emerging thermal management requirements identified in [17] should be adequately addressed. If these requirements are not met, SiPs become challenging to control. Moreover, their high fabrication costs make it impractical to equip SiPs with many temperature sensors. Adding these sensors would further increase the fabrication cost. Thus, there is a need to minimize the number of embedded temperature sensors. In addition, to minimize the time to market, SiPs are preferably based on existing chip-scale packaged ICs with only minor or no modifications. In contrast, packaging houses adopt thermal modeling techniques such as the finite element method (FEM) to provide the optimal combination of features [18], [19].

The contributions of the present paper are: (1) a Novel Peak-Source-Scanning (NPSS) algorithm for thermal management and monitoring of SiPs, (2) conducting numerical simulations based on MATLAB® tools to validate the efficiency of NPSS in detecting and managing up to six on-chip heat sources, (3) proving that NPSS is simple, fast, efficient, and easy to implement, without risk of ''rapid self-overheating,'' and (4) testing NPSS's efficiency in thermal management by proving its ability to detect accurately the number of on-chip heat sources as well as their respective positions and induced temperature distributions.

The rest of this paper is organized as follows: Section II describes the NPSS algorithm based on the Gradient Direction Sensors (GDS) method, Section III reports thermal simulation results confirming the validity of the NPSS algorithm, and Section IV discusses the obtained simulation results. This section also provides a comparison between Tp, the temperature predicted by the NPSS algorithm, and Te, the temperature estimated by the FEM obtained with COMSOL. Finally, Section V summarizes the paper's main contributions and findings.

II. THE PROPOSED NPSS ALGORITHM

A. DESCRIPTION OF THE GDS METHOD

The Gradient Direction Sensors (GDS) method uses ring oscillator (RO) sensors arranged in equilateral triangles to detect temperature gradients around heat sources (Fig. 3). Each three-sensor cell provides angular information, which, combined with the distances between the sensors and the heat source, allows the estimation of the source's temperature. By calculating frequency variations and angles within these cells, the GDS method offers a precise thermal detection approach with fewer sensors, efficiently monitoring multiple heat sources.

The proposed NPSS algorithm is based on GDSs adapted for systems comprising multiple heat sources. Although thermal scanning is a relevant solution from an algorithmic point of view, a sensor array comprising many heat sensors per IC, as reported in [20] and [21], is not required.

Instead, with NPSS, the number of these sensors can be significantly scaled down while still monitoring and profiling the temperature of the entire package.

Fig. 1 shows the simulation flow used in this work to get a thermal profile of SiP.

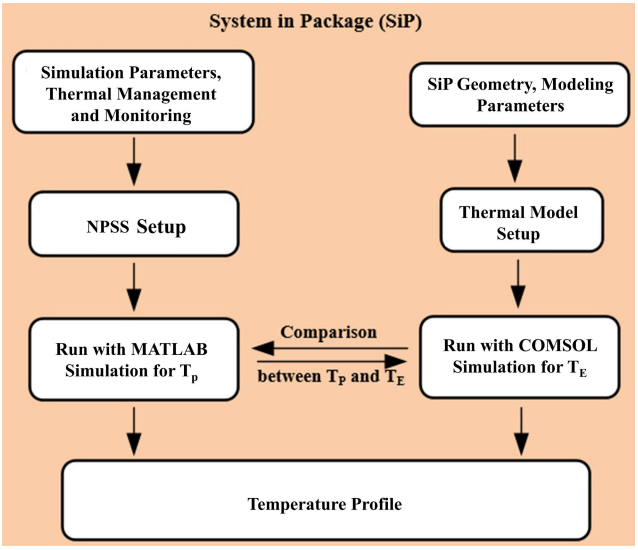

FIGURE 1. The proposed functional simulation and thermal modeling flow diagram for SiPs.

Fig. 2 shows a graphical summary of the key operations and results of the NPSS algorithm.

To generate our NPSS algorithm based on the GDS method, we propose using six ring oscillator (RO) sensors organized in two cells forming equilateral triangles, as shown in Fig. 3. This configuration allows the detection of thermal peaks in each of these three-sensor cells.

We must calculate the distance between the sensor and the designated source to obtain the temperature induced by a single localized heat source. The two 3-sensor cells are required for this purpose. The two cells are placed at a given distance (H) from each other, and each cell provides information about an angle α pointing in the direction of the heat source, as presented in Fig. 3(a) that depicts the construction of the proposed 3-sensor cell with $0° \leq \alpha \leq 60°$.

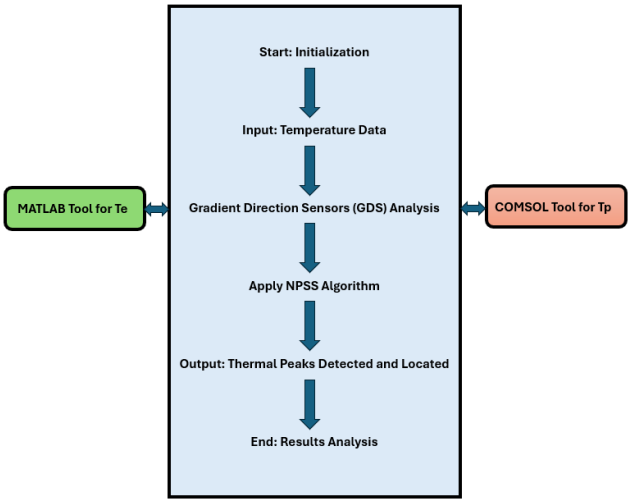

FIGURE 2. Graphical summary of operations and Key results of the NPSS algorithm.

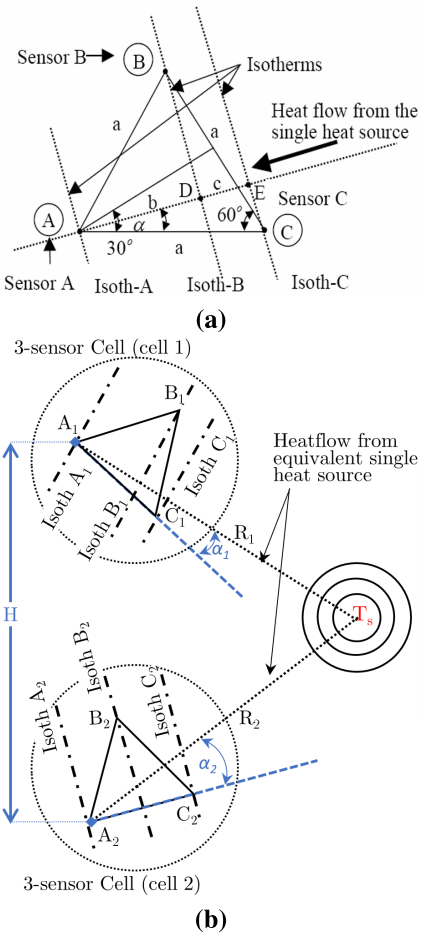

FIGURE 3. The GDS method: (a) the proposed 3-sensor cell, and (b) the overall topology showing the positions of the two 3-sensor cells with respect to the heat source.

Fig. 3(b) depicts the GDS method when it is used for detecting a single heat source (T_s). For each of the RO sensors, we assume that we have its node number and node coordinates as needed by the FEM model. Therefore, by calculating the temperature gradient along the known distance (H) between the 2 reference points (A_1 and A_2), and the distances (R_1 and R_2) to the heat source (T_s), we can estimate the temperature of the heat source. Assuming that the two sensor cells of Fig. 3(b) (cell 1 formed by the sensors A_1, B_1 and C_1, and cell 2 formed of the sensors A_2, B_2 and C_2) are placed in two corners of a monitored layout at the distance H from their reference points, the temperature of the heat source can be obtained by applying equation (1).

The isotherms of cell 2 in Fig. 3(b) are indeed not perpendicular to R2, unlike those of cell 1. This difference arises from the orientation of the heat source relative to each cell, which causes thermal gradients to vary according to the location of the collector. In particular, the non-perpendicularity in cell 2 results from the complex interactions between the heat source and the surrounding environment, which is accurately modeled by the NPSS algorithm. With regard to limiting the angle to $0° \leq \alpha \leq 60°$, it's important to note that this range allows us to effectively capture critical temperature gradients between sensors. To cover the area on both sides, we rely on several three-sensor cells positioned at different locations, ensuring complete coverage of the entire surrounding area.

In equation (1), the arrow $\rightarrow$ does not indicate a strict equality, but rather a process leading to an estimation of the temperature of the heat source, denoted as T_s. In other words, this equation is not used to calculate T_s exactly as an equality, but rather to deduce or estimate this temperature based on the frequencies obtained from the sensors and the calculated angles. The symbol $\rightarrow$ represents the transition from frequency to temperature, based on the temperature gradient we obtain by using the distances between the sensors and the heat source. In summary, the equation models the relationship between the measured parameters (frequencies and angles of the sensors) and the temperature of the heat source. We use this relationship to obtain an approximation of T_s, but it is not a direct equality.

$$\frac{\frac{H}{a}(f_{C_1} - f_{A_1})(\sqrt{3} + \tan\alpha_2)(1 + \tan\alpha_1^2)}{\sqrt{3}(1 - \tan\alpha_1 \tan\alpha_2) - (\tan\alpha_1 + \tan\alpha_2)} + f_{A_1} \rightarrow T_s \quad (1)$$

f_X represents the frequency obtained from a single Ts heat source using the GDS method, H is the distance between the reference sensors of the two cells of Fig. 3(b), a is the side length of the equilateral triangle shown in Fig. 3(a), and the angles α_1 and α_2 correspond to the two 3-sensor cells shown in Fig. 3(b) with $\tan(\alpha_i)$ being defined by the following equation:

$$\tan(\alpha_i) = \frac{2(f_{B_i} - f_{A_i})}{\sqrt{3}(f_{C_i} - f_{A_i})} - \frac{1}{\sqrt{3}} \quad (2)$$

The RO-type sensors (ring oscillators) are shown in Fig. 3, located at the vertices of each triangle. This configuration

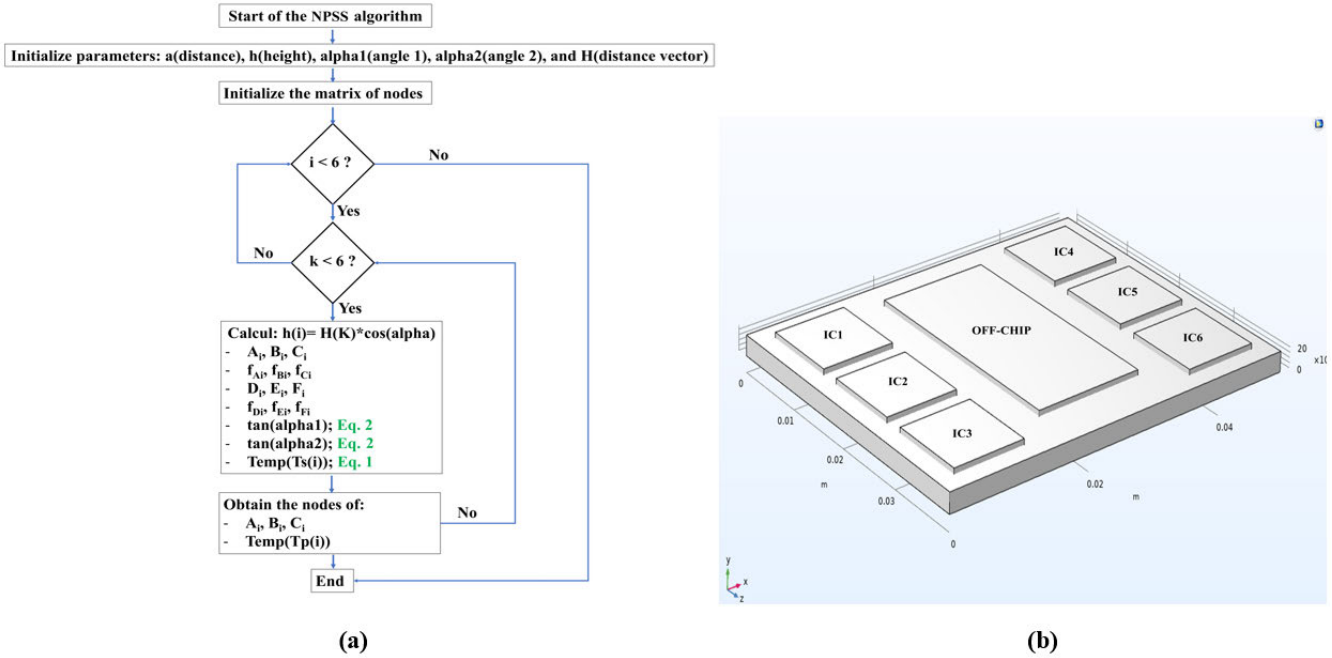

FIGURE 4. An illustration of the: (a) NPSS algorithm flowchart, and (b) geometry of the SiP model under study.

is applied directly to each integrated circuit (IC1 to IC6) in Fig. 4(b) to detect the temperature of each heat source, which corresponds to each IC in this case. The numbers on the axes in Fig. 4(b) represent the sizes and dimensions used by the COMSOL tool for the ICs, providing an understanding of how the analysis is conducted using this tool. Regarding Fig. 4(b), for each sensor i shown, the NPSS calculates the required parameters (temperatures and angles) to apply equation (2) between the designated sensor i and its neighboring sensors, identified as k in the Figure. These calculations are critical for estimating the temperatures based on the spatial relationships between the sensors.

B. THE FLOWCHART OF NPSS

As aforementioned, the NPSS algorithm is designed to scan all areas (and ICs) near the thermal detection cells and detect MHSs in each IC. It can accurately estimate the locations of all thermal peaks, i.e., areas on SiP with high temperatures. This can be achieved by applying the NPSS algorithm flowchart presented in Fig. 4(a). The algorithm starts by initializing all the required parameters and then loops over all SiP ICs. For this paper, we tested NPSS on the SiP presented in Fig. 4(b). Thus, we set the maximum number of ICs on SiP (the i parameter in Fig. 4 to 6. For every i, NPSS computes the required parameters (temperatures and angles) to apply equation (2) between the designated sensor i and all other neighboring sensors (identified by k in Fig. 4).

The NPSS can be generalized to MHSs, i.e., not limited to 6 heat sources. Such a property represents an advantage for NPSS over other traditional approaches ([22], [23]). With the current MATLAB implementation that will be demonstrated in later sections, NPSS converged rapidly, providing us with a proper time window to intervene and protect the SiP under study from extreme temperature conditions. This time window can be further maximized by accelerating NPSS's implementation using high-speed hardware, such as FPGAs. Hence, another advantage of NPSS over its competitors is its speed for an adequate prediction of on-chip thermal peaks during run-time since, to the best of our knowledge, other scanning algorithms do not yet support such a characteristic.

C. GEOMETRY OF THE SIP MODEL UNDER STUDY

Fig. 4(b) corresponds to an image imported from COMSOL Multiphysics showing the SiP's geometry to be analyzed by the NPSS algorithm and the zones' locations with their respective ICs. The considered SiP is equipped and assembled in a matrix of six ICs connected to the package and to each other via bonding wires. According to the flowchart presented in Fig. 4(a), the algorithm detects all thermal peaks sequentially, i.e., one thermal peak per loop starting with the zone (i=0, IC1) until reaching the zone (i=5, IC6) while incrementing i with a step of 1 after every iteration.

Fig. 5 provides a block diagram of the target SiP, showing how its modules are connected. The labels of the modules DI, GD, RM, DC-DC, ADC, and OFF-CHIP are respectively derived from their main functionality: Digital Isolation, Gate Driver, Readback Monitoring, DC to DC Converter, Analog to Digital Converter, and the module labeled OFF-CHIP module is the zone where various off-chip components are located. Early analysis indicates that the ICs needed in each module of the target system have different power dissipation. Table 1 summarizes some key module parameters depicted

in Fig. 4(b). The table highlights different IC dimensions (the areas in mm^2) and their respective power dissipation (in mW).

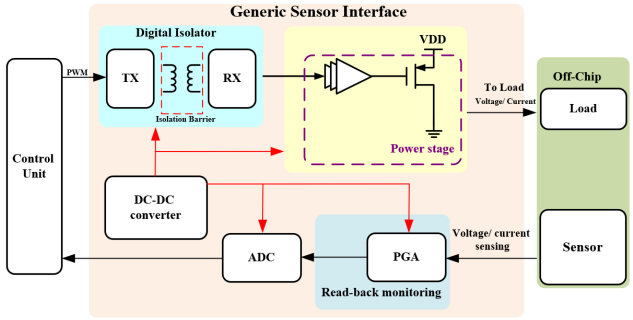

FIGURE 5. Generic SiP-based sensor interface.

Fig. 5 illustrates a block diagram of the SiP (System-in-Package) sensor interface, showing the interconnection of its various modules. The figure's labels - DI, DC-DC, ADC and OFF-CHIP - are derived from their main functions: Digital Isolation (DI), Gate Driver (GD), DC-DC converter, Analog-to-Digital Converter (ADC) and the OFF-CHIP section, which represents the area where external components are integrated. The legend refers to the sensor interface, as it details how the sensor interacts with other system components via these modules. The Figure gives an overview of how each element functions within the target SiP, allowing an understanding of the overall power dissipation and connectivity of the design.

The OFF-CHIP section in Fig. 5 refers to the area where various off-chip components are integrated, which may include sensors and additional circuitry that are not part of the main chip. While the labels Load and Sensors indicate these components, the focus of thermal monitoring is primarily on the modules within the chip, such as Digital Isolation (DI), Gate Driver (GD), and others. The reason the off-chip components are not thermally monitored in this design is that they generally have different power dissipation characteristics compared to the integrated circuits (ICs) on the chip. Table 1 outlines the key parameters of the on-chip modules, highlighting their power dissipation, which is crucial for thermal management. In contrast, the off-chip components may not contribute significantly to the overall thermal dynamics being monitored in this initial stage of analysis. This focus allows for a more streamlined approach to managing thermal performance within the primary ICs, ensuring the reliability and efficiency of the sensor interface.

TABLE 1. ICs with their power consumption and spacing between them.

Packaged ICs	Power (mW)	Area (mm^2)
IC1 (DI:Digital Isolation)	12	10
IC2 (DI:Digital Isolation)	64	10
IC3 (GD:Gate Driver)	12	10
IC4 (RM:Readback Monitoring)	12	10
IC5 (DC-DC:DC to DC Converter)	72	10
IC6 (ADC:Analog to Digital Converter)	20	10
OFF-CHIP	15	80

The modules in Table 1 will be labeled as follows: IC1: DI (Digital Isolation); IC2: DI (Digital Isolation); IC3: GD (Gate Driver); IC4: RM (Readback Monitoring); IC5: DC-DC (DC to DC Converter); IC6: ADC (Analog to Digital Converter). This labeling will enhance the understanding of how each IC functions within the SiP system and provide clearer associations between the modules and their respective components.

TABLE 2. Physical properties of various significant materials in the modeled SiP.

Material	$\rho(Kg/m^3)$	k(W/m.K)	Cp(J/Kg.K)	E(MPa)
Copper	8700	400	385	$1.1E^5$
Solder	7370	75	220	$5.4E^4$
Aluminium	2700	238	900	$7.0E^4$

Table 2 summarizes the properties and materials used for finite element thermo-mechanical modeling with COMSOL Multiphysics® [24], [25]. These physical properties were extracted from the COMSOL library. The following heat conduction equation (3) or energy conservation law applies in a transient regime. It is obtained by considering the heat flow equilibrium inside SiP's body:

$$\nabla.(k\nabla T) + Q = \rho C_p \frac{\partial T}{\partial t} \tag{3}$$

where T is the temperature, k represents the thermal conductivity, ρ and C_ρ high-speedass density of the material and specific heat capacity, respectively. The density type used in our case describes a bulk density whose thermal sensitivity is distributed throughout the SiP. In our case, it's the mass per unit volume of a substance. To simplify obtaining thermal maps, we assume the ambient temperature to be constant at 25 °C around the structure. Furthermore, the NPSS algorithm was optimized to reduce time complexity by reducing the total number of iterations inside its loop. The NPSS time complexity is $O(n)$ Where n is the number of heat sources, which is 6 in our case.

III. SIMULATION RESULTS

A. HEAT TRANSFER SOLVERS AND THERMAL ANALYSIS OF SIP

This section presents our numerical simulations used to analyze the temperature distribution, the low average temperature of the heated surfaces, the effects of pressure drop, and other thermo-mechanical phenomena that might occur in SiP. These analyses were performed using the CFD (Computational Fluid Dynamics) and FEM (Finite Element Method) tools. Both tools use dedicated pre- and post-processing tools. COMSOL Multiphysics® is a numerical simulation software based on the FEM method that is commonly used as a general heat transfer solver [26].

Fig. 6 shows the SiP's geometry modeled in COMSOL with its mesh. With this geometry and the heat transfer mechanisms, we can model the adopted SiP as a 2-D mesh that applies to in-plane thermal problems and integrates better with the NPSS algorithm. Considering that the heat

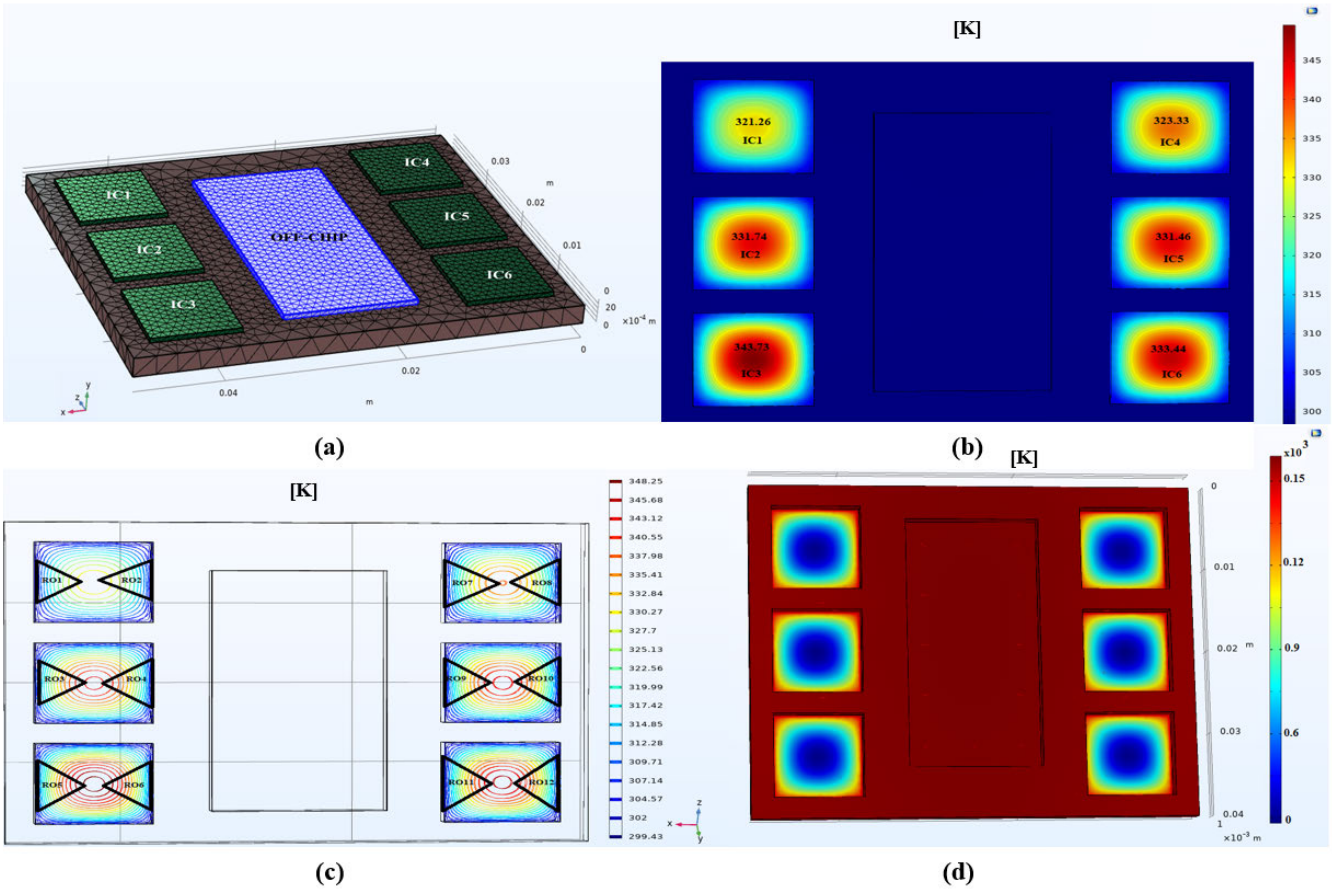

FIGURE 6. (a) Mesh used for the geometry of the SiP module adopted in COMSOL; (b) The temperature distribution of the six heat sources (full model with six ICs) (c); Prototype model built to validate the GDS method with six ICs; (d) The maximum stress distribution of the six heat sources.

will spread in the plane of the whole geometry and that an isothermal profile is necessary to perform a preliminary evaluation of the peak thermal value, a peak-value evaluation for the thermo-mechanical stresses becomes possible.

B. SIMULATION OF THE ADOPTED SIP MODULE WITH THE COMSOL TOOL

The COMSOL Multiphysics finite element analysis tool was used to estimate the thermal behavior of the adopted SiP. Using this tool, various thermal boundary conditions can be applied in both transient and steady-state analyses. Setting the thermal boundary conditions is challenging, especially when modeling thermal phenomena in SiPs. It mainly depends on the following three factors:

(i) The cooling method;
(ii) The position of the dissipated power and the influence of their surroundings;
(iii) The thermal conductivity of the materials in the SiP.

The thermal behavior of a SiP, with the modeled geometry shown in Fig. 6(a), is obtained by applying a set of partial differential equations and boundary conditions. The finite element method transforms partial differential equations into algebraic equations. This allows temperature stress analysis to be performed at different points or nodes in the model. However, the vertical boundary condition represents a big problem for numerical simulations. The most straightforward approach is to fix the ambient temperature of the structure at a constant value (for example, at 25 °C or 298.15 K) to produce a thermal short circuit. To solve the thermal equations, the boundary conditions must be defined.

Fig. 6(b) shows the results of a thermal simulation of the modeled SiP with six heat sources (one in each of six ICs) using COMSOL. Simulating the complete SiP module with COMSOL Multiphysics® gives a good estimate of the thermal diffusion of heat generated by the six sources. Fig. 6(b) shows the maximum temperature at 71.85 °C (345 K), which gives a good indication of the global thermal map.

To apply the NPSS algorithm, we use the GDS method, and we proceed by implementing a set of RO sensors in the form of cells of six RO sensors, which are positioned according to a configuration of two equilateral triangles whose ends are provided with one sensor each. Thus, a total of 6 sensors are needed in each IC for a total of 36 temperature sensors in the modeled SiP. This configuration of RO sensor cells allows GDS to be applied to detect thermal peaks in the proximity

of these RO cells, thus extending the application of GDS to detect multiple heat sources in the ICs.

The black triangles in Fig. 6(c) indeed represent the locations of the sensors. These sensors are strategically positioned to monitor critical points of the infrastructure, enabling early detection of anomalies such as temperature variations or abnormal vibrations. Their placement aims to optimize coverage and measurement accuracy, particularly in areas prone to accelerated deterioration.

Fig. 6(c) shows the prototype built to use the GDS method. The figure shows the heat map of the SiP model with a maximum temperature of 74.85 °C (348.25 K) observed at the center of the IC. This benchmark was developed to validate the GDS method with the six ICs.

Fig. 6(d) shows the thermal stress distribution obtained with the COMSOL model based on these equations. This distribution notably allows finding the maximum stress value. According to the figure, the maximum reported stress is 150 MPa, which is respectively close to the number obtained through the analytical method (results obtained by solving equations (4 and 5) in the Maple software).

C. STRESS ANALYSIS OF THE SIX HEAT SOURCES

To demonstrate the importance of FEM analyses such as COMSOL Multiphysics®, we will compare the analytical method with the thermal stress level of our SiP model. According to the Saint-Venant principle, the dominant stress generated by a heat source is generally found near the peak of the thermal stress. For each heat source, the exponential expressions that satisfy the tendency for the normal and shear stress distributions are expressed in equations (4 and 5) as follows:

$$\sigma(x) = \frac{1}{S}(N \sum_{i=1}^{3} R_i T_i c_{i1} e^{-R_i x} + M \sum_{i=1}^{3} R_i T_i c_{i2} e^{-R_i x}) \quad (4)$$

$$\tau(x) = \frac{1}{S}(N \sum_{i=1}^{3} R_i c_{i1} e^{-R_i x} + M \sum_{i=1}^{3} R_i c_{i2} e^{-R_i x}) \quad (5)$$

Here's an explanation of the quantities used in equations (4) and (5), with proper formatting for the indices:

- $\sigma(x)$ and $\tau(x)$ represent the normal and shear stress at a position x within the SiP structure. - S is a scaling factor related to the material properties and dimensions of the SiP. - N and M are constants that reflect the relative contributions of different modes of stress from the heat sources. - R_i is the thermal resistance of the i heat source, which affects the stress distribution. - T_i is the temperature of the i heat source. - c_{i1} and c_{i2} are coefficients related to the material and geometric properties that influence the exponential decay of stress. - $e^{-R_i x}$ represents the exponential decay of stress along the distance x from the heat source.

These two equations are used to estimate the stress distribution and thermal stress in the SiP structure.

The model used to derive equations (4) and (5) is based on the principles of thermal stress analysis, specifically applying the Saint-Venant principle. This principle states that the dominant stress from a heat source is generally localized near the peak thermal stress.

In equations (4) and (5), $\sigma(x)$ and $\tau(x)$ represent the normal and shear stresses within the System-in-Package (SiP) structure, respectively. The parameters involved, such as thermal resistance (R_i), temperatures (T_i), and coefficients (c_{i1} and c_{i2}), are crucial for modeling the stress distribution caused by heat sources. While section C and Fig. 7 may appear somewhat peripheral to the main topic, they are integral to demonstrating the comparative effectiveness of our analytical method against finite element method (FEM) analyses, specifically using COMSOL Multiphysics®. Fig. 7 provides a visual representation of the thermal stress distributions, allowing for a clear comparison between the results obtained from both methods. This comparison highlights the relevance of the equations in assessing thermal behavior within the SiP.

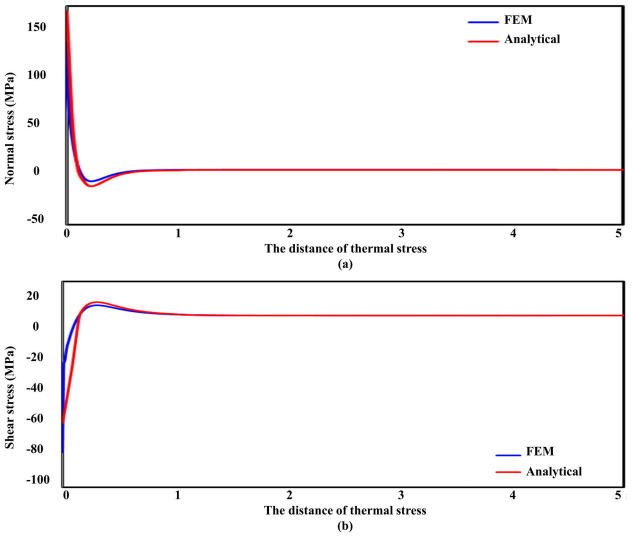

FIGURE 7. Thermal stress for the whole modulus: (a) Comparison of normal thermal stress analysis by FEM and analytical method; (b) Comparison of thermal shear stress analysis by FEM and analytical method.

Fig. 7 shows the results of the normal and shear-stressed thermal distributions by the FEM method as compared to the ability of the analytical method. The comparison results of the normal distribution are shown in Fig. 7(a), whereas those for the shear stress distribution are presented in Fig. 7(b). Typically, SiPs with thermal risks or availability considerations consist of high-speed logic arrays.

D. MATLAB NUMERICAL IMPLEMENTATION OF NPSS

A MATLAB® numerical implementation of the NPSS algorithm was successfully executed. It comprises the following steps:

1) Predicting the thermal monitoring zone area;
2) Selecting the characteristics of the six ROs sensor cell configuration;

3) Calculating the coordinates of the sensors in each cell;
4) Detecting the temperatures of the sensors;
5) Calculating Tp, and
6) Calculating the coordinates of the sensors of all cells without approximations.

In addition to respecting the execution steps in MATLAB® and the NPSS algorithm, we ensured that the two RO triangles did not touch each other (see Fig. 6(c)).

Fig. 8 shows the maximum temperature predicted (Tp) by our NPSS algorithm for IC1 to IC6. Based on Fig. 8 and Fig. 6(b), we calculated the maximum error between the thermal values predicted by our NPSS algorithm and those estimated with the COMSOL Multiphysics®.

Performing a detailed analysis of the thermal response of the NPSS algorithm illustrated in Fig. 8 will allow us to better understand its behavior in real environments, take appropriate measures to compensate for thermal variations, and optimize its overall performance.

This Figure illustrates the maximum temperature predicted (Tp) by our NPSS algorithm for integrated circuits (IC1 to IC6). It is important to note that the temperatures represented correspond to the estimated maximum values during the operational phase of the circuits. While these temperatures may fluctuate over time due to varying operational conditions, our NPSS algorithm is designed to estimate these maximum values, which are crucial for assessing thermal performance. Moreover, the algorithm does not experience a time delay in obtaining these values, although it does have a response time of approximately $\tau_r = 0.34$ *seconds*. This means that after a thermal variation, the algorithm requires this time to adapt and stabilize its outputs, which is critical for analyzing its effectiveness in real-world scenarios where thermal conditions can change rapidly. In our analysis of the thermal response presented in Fig. 8, we considered several key aspects. First, we studied the thermal sensitivity, finding that approximately 45 % of the predicted temperatures aligned with actual measurements, highlighting the algorithm's sensitivity to thermal variations. Next, we evaluated the response time of the NPSS algorithm, measured at 0.34 *seconds*, to understand how quickly it can adapt after a temperature change. Additionally, our analysis identified that the algorithm operates reliably within a temperature range of 343.73 K to 345.00 K. Furthermore.

Table 3 compares the predicted and estimated temperatures for the different integrated circuits, shows a maximum error of approximately 1.27 K, validating the accuracy of our NPSS algorithm.

Thermal tolerance refers to the range of temperatures within which the NPSS algorithm operates reliably. In our analysis, we observed that the algorithm maintains its accuracy and performance within a temperature range of 343.73 K to 345.00 K, beyond which there might be a reduction in predictive accuracy. This tolerance range is crucial for determining the operational limits of the algorithm in real-world scenarios.

In the context of our NPSS algorithm and the comparison with COMSOL Multiphysics®, the heat sources for each IC represent the power dissipation levels during their operation, which directly influence the predicted and estimated temperatures. The temperatures T_p (predicted) and T_e (estimated) shown in the table are the maximum values obtained under operational load conditions for each IC. These are the critical temperatures reached when the ICs are subjected to maximum power dissipation, allowing us to evaluate the accuracy of the NPSS algorithm in predicting thermal peaks.

We compare our proposed NPSS algorithm with other schemes presented in the literature. Table 4 shows the SiP modeling using three models, including our NPSS algorithm and two methods used in [27] and [28]. Other works were validated by simulations only (with different objectives) without regard to theoretical models or algorithms. To the best of our knowledge, we are the first to propose a new method based on an advanced algorithm capable of detecting the thermal peaks for all ICs in a SiP and characterizing their thermal behaviors.

TABLE 3. Comparison between our NPSS algorithm and the COMSOL Multiphysics® in terms of temperature parameters of each IC's heat source.

Heat sources	IC1	IC2
Temperature Tp (K)	321.55	332.03
Temperature Te (K)	321.26	331.74
Error Rates (K)	0.29	0.29
Heat sources	IC3	IC4
Temperature Tp (K)	345.00	323.62
Temperature Te (K)	343.73	323.33
Error Rates (K)	1.27	0.29
Heat sources	IC5	IC6
Temperature Tp (K)	331.75	333.73
Temperature Te (K)	331.46	333.44
Error Rates (K)	0.29	0.29

TABLE 4. Comparison of SiP modeling with NPSS algorithm and with comparable works.

References	Proposed	[27]	[28]
Method	NPSS[(a)]	TIM[(b)]	ETC[(c)]
Temperature (K)	345.00	376.30	339.15
Error (K)	1.27	2.31	2.80

[(a)] Novel Peak-Source-Scanning (NPSS);
[(b)] Thermal Interface Material (TIM);
[(c)] Electro-Thermal Coupling (ETC).

Table 4 reports a maximum error value (1.27 K) for our NPSS algorithm. Thus, our NPSS algorithm outperforms the Thermal Interface Material (TIM) and the Electro-Thermal Coupling (ETC) methods. No out-of-range values are observed, especially for temperatures between 298 K and 304 K.

Following the comparative results in Tables 3 and 4, we deduce that our proposed NPSS is a good and accurate solution that is easy to implement and has low computational complexity. The NPSS's computation time depends on the algorithmic complexity, the size of the input data, and the

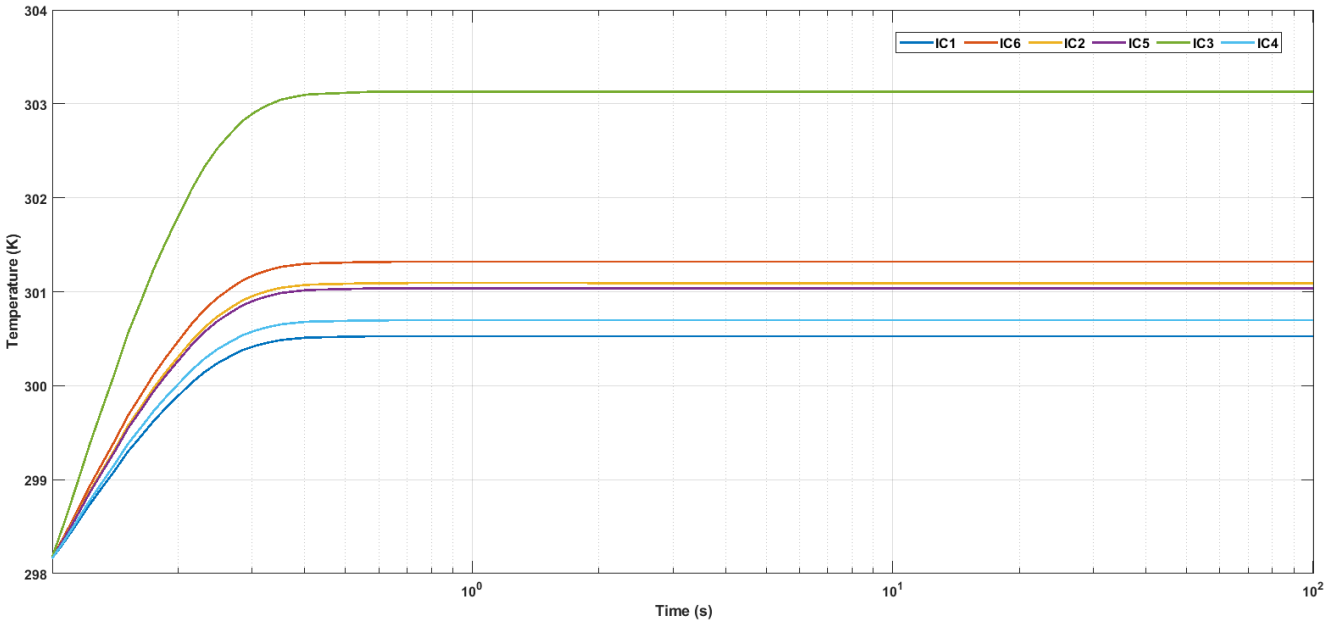

FIGURE 8. Maximum temperature predicted and generated by the NPSS algorithm for (IC1 to IC6).

testing hardware. In our case, the overall simulation time was 46.819 *seconds* using a 6-CPU x86_64 Windows 10 computer with a clock speed of 3.2 GHz.

As mentioned, faster execution is possible with dedicated implementations, which we will explore in our future work. Nonetheless, the current MATLAB implementation of NPSS is respectively fast for some real-time thermal monitoring applications. In addition, the proposed method does not introduce the risk of ''rapid overheating'' caused by the heat of the sensors that are added to the surface of the chips to measure the frequency variations generated by these sensors, indicating the thermal changes in the chip [29] and [30].

E. DISCUSSION: COMPARATIVE ANALYSIS OF THE NPSS ALGORITHM

In this section, we provide a detailed comparison of our Novel Peak Source-Scanning (NPSS) algorithm with existing methods to highlight its advantages. Using simulation tools like COMSOL Multiphysics® and MATLAB®, we evaluated NPSS's performance in detecting and locating thermal peaks in System-in-Package (SiP) systems.

The Thermal Interface Material (TIM) method (Table 4), with a maximum temperature of 376.30 K and an error of 2.31 K, contrasts with NPSS, which achieves a maximum temperature of 345.00 K with an error of just 1.27 K, indicating superior accuracy. TIM is known for its increased complexity due to thermal interface optimization, while NPSS offers a more straightforward approach with fewer required sensors, thus reducing overall complexity. The Electro-Thermal Coupling (ETC) method (Table 4), showing a maximum temperature of 339.15 K with an error of 2.80 K, is outperformed by NPSS, demonstrating better precision with its lower error. ETC often requires frequent adjustments and calibrations, whereas NPSS provides a robust method with minimal error, enhancing reliability.

NPSS also reduces sensor requirements while maintaining precise monitoring, unlike existing methods that may need more sensors or complex systems. Additionally, NPSS executes in 46.8 *seconds* on a standard computer, making it suitable for real-time applications and avoiding the ''rapid overheating'' risk associated with added sensors on chip surfaces, as noted in previous studies.

The 46.8 *seconds* figure represents the total time required for the NPSS algorithm to compute the full thermal analysis for the entire System-in-Package (SiP), which includes six integrated circuits (ICs) and multiple heat sources. This computation accounts for not only the evaluation of equations (1) and (2) but also other complex steps such as iterative adjustments for boundary conditions, convergence checks, and fine-tuning based on real-time temperature fluctuations. While equations (1) and (2) themselves are simple to evaluate, the overall complexity of the system requires significant computational effort, especially when integrating multiple ICs and comparing results with finite element method (FEM) simulations. The goal of the paper is indeed to propose an efficient method GDS for predicting the peak temperature (Tp), and despite the total computation time, our method still provides more accurate and efficient results than conventional approaches in complex environments.

As for the 0.34 *seconds* response time, this refers specifically to the NPSS algorithm's ability to adapt to real-time thermal variations. After a temperature change occurs, the algorithm takes approximately 0.34 *seconds* to update its predictions and stabilize. This rapid response is

critical for real-time thermal management. The 46.8 *seconds*, on the other hand, reflect the initial full computation time required for the entire SiP analysis, which is performed once, whereas the response time is for dynamic, on-the-fly adjustments.

Regarding the processing power required, we do not suggest that each IC is equipped with an individual temperature monitor requiring 46.8 *seconds* of processing time on a Windows-based system. Instead, the thermal management system operates centrally, where these calculations are performed on more powerful hardware. Each IC relies on the centralized system for real-time updates and adjustments, ensuring efficient temperature control without excessive computational demands locally on the IC.

First, we confirm that the TIM and ETC methods were indeed implemented, but not within our exact hardware configuration. These methods were tested on similar systems, as referenced in [27] and [28], to benchmark their performance against NPSS. Although different systems were used, the comparison remains relevant due to the thermal behaviors we observed across comparable conditions, such as peak temperature and error rates. The methods used in the literature were carefully simulated to closely match our SiP structure in terms of operational parameters and thermal behavior, ensuring a fair comparison. This allows us to highlight NPSS's advantages in terms of precision, simplicity, and reduced error rate, as illustrated in Table 4. Regarding the discussion about the sensors and their integration into the chips, the phrase (heat sensors added to the surface of the chips) refers to the use of thermal sensors that monitor the chip's surface temperature in real-time. In our NPSS algorithm, the number of required sensors is minimized compared to TIM and ETC, which often require additional sensors and frequent re-calibration. These sensors are typically added at key thermal hots-pots across the chip's surface to monitor and record temperature variations more accurately. This approach reduces overall complexity while maintaining precise thermal management. Finally, Table 4's figures are derived from both simulation data and real-world measurements. The TIM and ETC methods, as reported in the literature, rely heavily on complex thermal interface configurations and electro-thermal coupling, which can introduce significant errors and require fine-tuning. In contrast, NPSS maintains lower error rates and better adaptability to real-time conditions without needing the same level of complexity or re-calibration.

In summary, NPSS excels in precision, simplicity, and efficiency compared to TIM, ETC methods (Table 4), making it particularly suitable for thermal management in high-density SiP systems. Future dedicated implementations could further improve execution speed, but the current NPSS version is already effective for real-time thermal monitoring applications.

IV. CONCLUSION AND FUTURE WORKS

This paper proposes a Novel Peak-Source-Scanning (NPSS) algorithm based on the Gradient Direction Sensor (GDS) method. NPSS can perform thermal management of Systems-in-Package (SiPs) that typically comprise multiple heat sources. We implemented the NPSS algorithm to detect thermal peaks in a SiP comprising six heat sources.

Compared to the present literature, our NPSS algorithm provides more accurate estimates of thermal peaks calculated using a reference FEM model available in COMSOL with a maximum error of 1.27 K observed between the predicted and estimated temperatures. The proposed algorithm also offers an excellent time complexity of $O(n)$. Moreover, our algorithm is a cost-effective solution for thermal management, as it requires a much lower number of sensors than the previously reported solutions.

Our study primarily focuses on the theoretical demonstration and simulation validation of the NPSS algorithm, aiming to present a robust proof of concept and validate the algorithm's feasibility and effectiveness in a controlled environment before considering more extensive experimental validations. Our study provides a solid theoretical foundation for future practical integration and optimization work. While our paper focuses on algorithmic validation, we understand the importance of compatibility and financial implications, which will be addressed in future studies once the algorithm's validity and benefits have been demonstrated through simulations.

Experimental validation, although crucial, requires considerable resources and a specific framework that goes beyond the scope of our current study. However, our simulations were designed to replicate realistic conditions and provide clear indications of the algorithm's performance, thus demonstrating its initial viability. Additionally, we included comparisons with relevant simulation benchmarks and plan to include comparisons with physical implementations in future work.

We firmly believe that the simulation validation presented in this paper is a crucial step for the initial demonstration of the NPSS algorithm.

Our future works will explore temperature measurement accuracy and computational complexity when implementing NPSS in C/C++ and studying its performance in terms of portability and real-time monitoring of thermal management for different SiP configurations. We also plan to implement NPSS in SiP devices for in-situ real-time thermal management.

REFERENCES

[1] J. H. Lau, "Recent advances and trends in advanced packaging," *IEEE Trans. Compon., Packag., Manuf. Technol.*, vol. 12, no. 2, pp. 228–252, Feb. 2022, doi: 10.1109/TCPMT.2022.3144461.

[2] J. H. Lau, "Recent advances and trends in multiple system and heterogeneous integration with TSV-less interposers," *IEEE Trans. Compon., Packag., Manuf. Technol.*, vol. 12, no. 8, pp. 1271–1281, Aug. 2022, doi: 10.1109/TCPMT.2022.3194374.

[3] X. Liu, W. Zhang, D. Hao, and Y. Liu, "Differential-fed magneto-electric dipole antenna with integrated balun based on ball grid array packaging," *IEEE Trans. Compon., Packag., Manuf. Technol.*, vol. 12, no. 6, pp. 981–987, Jun. 2022, doi: 10.1109/TCPMT.2022.3165595.

[4] J. Chen, X. Meng, R. Zhou, K. Lu, Y. Jin, and S. Zheng, "A compact on-chip pad structure with an embedded capacitor for broadband millimeter-wave bond-wire interconnection," *IEEE Trans. Compon., Packag., Manuf. Technol.*, vol. 12, no. 12, pp. 1949–1958, Dec. 2022, doi: 10.1109/TCPMT.2022.3218593.

[5] H. Li, Y. Kong, H. Huang, and Y. Zhang, "Integrated electronic system of spacecraft based on SiP technology," in *Proc. IEEE 13th Int. Conf. Signal Process. (ICSP)*, Chengdu, China, Nov. 2016, pp. 1809–1812, doi: 10.1109/ICSP.2016.7878140.

[6] S. S. Salvi and A. Jain, "A review of recent research on heat transfer in three-dimensional integrated circuits (3-D ICs)," *IEEE Trans. Compon., Packag., Manuf. Technol.*, vol. 11, no. 5, pp. 802–821, May 2021, doi: 10.1109/TCPMT.2021.3064030.

[7] A.-C. Iradukunda, D. R. Huitink, and F. Luo, "A review of advanced thermal management solutions and the implications for integration in high-voltage packages," *IEEE J. Emerg. Sel. Topics Power Electron.*, vol. 8, no. 1, pp. 256–271, Mar. 2020, doi: 10.1109/JESTPE.2019.2953102.

[8] S. Reich, M. Sporer, M. Haas, J. Becker, M. Schüttler, and M. Ortmanns, "A high-voltage compliance, 32-channel digitally interfaced neuromodulation system on chip," *IEEE J. Solid-State Circuits*, vol. 56, no. 8, pp. 2476–2487, Aug. 2021, doi: 10.1109/JSSC.2021.3076510.

[9] J. Gao and J. B. Kwak, "Reliability and thermal fatigue life prediction of solder joints for advanced automotive microelectronics," *J. Mech. Sci. Technol.*, vol. 35, no. 8, pp. 3633–3641, Aug. 2021, doi: 10.1007/s12206-021-0734-6.

[10] S. F. Choudhury and L. Ladani, "Effect of intermetallic compounds on the thermomechanical fatigue life of three-dimensional integrated circuit package microsolder bumps: Finite element analysis and study," *J. Electron. Packag.*, vol. 137, no. 4, pp. 1043–7398, Dec. 2015, doi: 10.1115/1.4031523.

[11] L. J. Ladani, "Numerical analysis of thermo-mechanical reliability of through silicon vias (TSVs) and solder interconnects in 3-dimensional integrated circuits," *Microelectronic Eng.*, vol. 87, no. 2, pp. 208–215, Feb. 2010, doi: 10.1016/j.mee.2009.07.022.

[12] A. Oukaira, O. Ettahri, and A. Lakhssassi, "Modeling and FPGA implementation of a thermal peak detection unit for complex system design," *Int. J. Adv. Comput. Sci. Appl.*, vol. 8, no. 6, pp. 307–312, 2017, doi: 10.14569/ijacsa.2017.080640.

[13] M.-K. Shih, N.-Y. Wu, W.-H. Lai, T.-Y. Chen, C.-L. Kao, and C. P. Hung, "Board-level drop impact reliability analysis of dual-side molding system-in-package (SiP) modules," *IEEE Trans. Electron Devices*, vol. 70, no. 1, pp. 215–221, Jan. 2023, doi: 10.1109/TED.2022.3223632.

[14] W. Wang, Z. Jia, J. Zhang, and H. Li, "Multi-chip coupling thermal resistance topological network model and chip junction temperature prediction of system in package," *Heat Transf. Res.*, vol. 54, no. 1, pp. 57–75, 2023, doi: 10.1615/heattransres.2022044334.

[15] M. John and K. Shankar, "A review on transient thermal management of electronic devices," *ASME J. Electron. Packag.*, vol. 144, no. 1, 2022, Art. no. 010801, doi: 10.1115/1.4050002.

[16] G. Baek and H. Jeong, "All-digital time-domain temperature sensor for energy efficient on-chip thermal management," in *Proc. Int. Conf. Electron., Inf., Commun. (ICEIC)*, Feb. 2022, pp. 1–4, doi: 10.1109/ICEIC54506.2022.9748344.

[17] R. Ghaffarian, "Assembly reliability of eWLP, die- and die-size BGA," in *Proc. 21st IEEE Intersociety Conf. Thermal Thermomechanical Phenomena Electron. Syst. (iTherm)*, San Diego, CA, USA, May 2022, pp. 1–9, doi: 10.1109/iTherm54085.2022.9899504.

[18] X. Konstantinou, J. D. Albrecht, P. Chahal, and J. Papapolymerou, "Flexible chip-first millimeter-wave packaging using multiple dielectrics," *IEEE Trans. Compon., Packag., Manuf. Technol.*, vol. 12, no. 4, pp. 682–691, Apr. 2022, doi: 10.1109/TCPMT.2022.3160626.

[19] A. Bocca and A. Macii, "Thermal modeling and analysis of a power ball grid array in system-in-package technology," *Multiscale Multidisciplinary Model., Exp. Des.*, vol. 5, no. 1, pp. 31–41, Mar. 2022, doi: 10.1007/s41939-021-00101-w.

[20] Y. Lai, K. Pan, C. Cai, P. Yin, J. Yang, and S. Park, "Smarter temperature setup for reflow oven to minimize temperature variation among components," *IEEE Trans. Compon., Packag., Manuf. Technol.*, vol. 12, no. 3, pp. 562–569, Mar. 2022, doi: 10.1109/TCPMT.2022.3153952.

[21] A. Lakhsasi, M. Bougataya, and D. Massicotte, "Practical approach to gradient direction sensor method in very large scale integration thermomechanical stress analysis," *J. Vac. Sci. Technol. A, Vac., Surf., Films*, vol. 24, no. 3, pp. 758–762, May 2006.

[22] A. Oukaira, D. Said, J. Zbitou, and A. Lakhssassi, "Finite element method for system-in-package (SiP) technology: Thermal analysis using chip cooling laminate chip (CCLC)," in *Proc. IEEE 17th Int. Conf. Ubiquitous Inf. Manage. Commun. (IMCOM)*, Sep. 2023, pp. 1–5, doi: 10.1109/IMCOM56909.2023.10035652.

[23] A. Oukaira, D. Said, J. Zbitou, and A. Lakhssassi, "Transient thermal analysis of system-in-package technology by the finite element method (FEM)," in *Proc. IEEE Int. Conf. Microelectron. (ICM)*, Jun. 2022, pp. 30–33, doi: 10.1109/ICM56065.2022.10005514.

[24] S. S. M. Ghoneim, M. Ahmed, and N. A. Sabiha, "Transient thermal performance of power cable ascertained using finite element analysis," *Processes*, vol. 9, no. 3, p. 438, Feb. 2021, doi: 10.3390/pr9030438.

[25] M. Eisele, Y. Hwang, and R. Radermacher, "Small-scale dynamic test facility for automotive thermal management systems," in *Proc. Vehicle Thermal Manage. Syst. Conf. Exhib. (VTMS)*, May 2011, pp. 523–535, doi: 10.1533/9780857095053.7.523.

[26] W.-L. Fan, X.-W. Gao, and B.-B. Xu, "Free element boundary integration method for solving heat conduction and mechanics problems," *Eng. Anal. With Boundary Elements*, vol. 148, pp. 104–113, Mar. 2023, doi: 10.1016/j.enganabound.2022.12.026.

[27] N. Goel, T. K. Anoop, A. Bhattacharya, J. A. Cervantes, R. K. Mongia, S. V. Machiroutu, H.-L. Lin, Y.-C. Huang, K.-C. Fan, B.-L. Denq, C.-H. Liu, C.-H. Lin, C.-W. Tien, and J.-H. Pan, "Technical review of characterization methods for thermal interface materials (TIM)," in *Proc. 11th Intersociety Conf. Thermal Thermomechanical Phenomena Electron. Syst.*, vol. 13, Orlando, FL, USA, May 2008, pp. 248–258, doi: 10.1109/itherm.2008.4544277.

[28] T. Xiong, X. Zhu, Y. Fang, and S. Long, "High performance finite element algorithm for electro-thermal coupling field based on high order elements," in *Proc. IEEE 5th Int. Conf. Electron. Technol. (ICET)*, Chengdu, China, May 2022, pp. 506–510, doi: 10.1109/ICET55676.2022.9825264.

[29] O. Ettahri, A. Oukaira, M. Ali, A. Hassan, M. Nabavi, Y. Savaria, and A. Lakhssassi, "A real-time thermal monitoring system intended for embedded sensors interfaces," *Sensors*, vol. 20, no. 19, p. 5657, Oct. 2020, doi: 10.3390/s20195657.

[30] S. Lopez-Buedo, J. Garrido, and E. I. Boemo, "Dynamically inserting, operating, and eliminating thermal sensors of FPGA-based systems," *IEEE Trans. Compon. Packag. Technol.*, vol. 25, no. 4, pp. 561–566, Dec. 2002, doi: 10.1109/TCAPT.2002.808011.

AZIZ OUKAIRA (Member, IEEE) received the Ph.D. degree in electrical engineering from Université du Québec en Outaouais, Gatineau, QC, Canada, in 2020. From 2020 to 2022, he was a Postdoctoral Fellow with the Polystim Neurotechnologies Laboratory, Department of Electrical Engineering, Polytechnique Montréal, Canada. He is currently a Professor with the Electrical Engineering Department, Université de Moncton. He is also affiliated with Université du Québec en Outaouais. His research interests include thermal management, rapid prototyping on FPGA, MEMS, microelectronics, thermal aspects in VLSI microsystems, biomedical signal modeling, extraction of thermal measurements, detection of heat zones invisible to the naked eye for surfaces of integrated systems, such as IC, SoC and SiP, and parallel architecture platforms for embedded systems.

DHAOU SAID (Member, IEEE) received the Engineering degree in electric engineering and the Master of Research degree in communication systems from the National School of Engineers of Tunis, and the Ph.D. degree (Hons.) in electrical and computer engineering from the Université de Sherbrooke, Canada, in December 2014, and the Ph.D. Diploma degree in network and computer science from the University of Technology of Troyes (UTT), France, in December 2014. He was a Postdoctoral Researcher, a Researcher, a Software Developer, a Manager, and a Mentor with the University of Ottawa. He is currently a Visionary and the Charismatic Leader of the Dynamic Research and Development Strategies, focused on technological innovations in data privacy and cyber-attack detection using quantum and AI/ML models. His research interests include quantum computing, cybersecurity, artificial intelligence, metaverse, blockchain technology, convergence and computing complexity reduction, the IoT, smart grid, and autonomous electric vehicle.

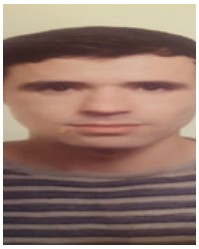

DJALLEL EDDINE TOUATI (Member, IEEE) received the M.Sc. degree in electrical engineering from the Department of Computer Science, University of Quebec, Montreal, QC, Canada, in 2016. He is currently pursuing the Ph.D. degree with the LIMA Laboratory, Université du Québec en Outaouais, in collaboration with the Polystim Neurotechnologies Laboratory, Department of Electrical Engineering, Polytechnique Montréal, Canada. His research interests include electrothermal characterization and reliability of electronic devices.

NADER EL-ZARIF (Member, IEEE) received the bachelor's degree in electronics and communications engineering from Beirut Arab University, Lebanon, in 2009, and the master's degree in electrical and computer engineering from the American University of Beirut, Lebanon, in 2012. He is currently pursuing the Ph.D. degree. He is a member of the GRM Laboratory, Polytechnique Montréal, Canada. His research interests include dc-dc converters, thermal modeling, machine learning, and wireless communications.

AHMAD HASSAN (Senior Member, IEEE) received the Ph.D. degree in electrical engineering from Polytechnique Montréal, Canada, in 2019. From 2019 to 2021, he was a Postdoctoral Fellow with the Polystim Neurotechnologies Laboratory, Department of Electrical Engineering, Polytechnique Montréal. From 2021 to 2022, he was a Postdoctoral Fellow with the Integrated Systems Laboratory, Department of Electrical and Computer Engineering, University of Toronto, Canada. He joined the Electrical Engineering Department, Polytechnique Montréal as an Assistant Professor, in 2023. During his research, he contributed to various research and industrial projects and has authored more than 55 research works in international journals and symposiums. His research is oriented towards emerging technologies including integrated circuits for harsh environments and photonic computing. He was a recipient of FRQNT Postdoctoral Research Scholarship.

YVON SAVARIA (Life Fellow, IEEE) received the B.Ing. and M.Sc.A. degrees in electrical engineering from École Polytechnique Montreal in 1980 and 1982, respectively, and the Ph.D. degree in electrical engineering from McGill University, in 1985. Since 1985, he has been with Polytechnique Montréal, where he is currently a Professor with the Department of Electrical Engineering. He has carried out work in several areas related to microelectronic circuits and microsystems, such as testing, verification, validation, clocking methods, defect and fault tolerance, effects of radiation on electronics, high-speed interconnects, and circuit design techniques, CAD methods, reconfigurable computing and applications of microelectronics to telecommunications, aerospace, image processing, video processing, radar signal processing, and the acceleration of digital signal processing. He is currently involved in several projects related to embedded systems in aircraft, wireless sensor networks, virtual networks, software-defined networks, machine learning (ML), embedded ML, computational efficiency, and application-specific architecture design. He holds 16 patents, has published 211 journal papers and 495 conference papers, and was the thesis advisor of 190 graduate students who completed their studies. He was the program Co-Chairman of NEWCAS'2018 and general Chairman of NEWCAS'2020. He has been working as a consultant or was sponsored for carrying out research with Bombardier, Buspass, CNRC, DesignWorkshop, Dolphin, DREO, Ericsson, Genesis, Gennum, Huawei, Hyperchip, Intel, ISR, Kaloom, LTRIM, Miranda, MiroTech, Nortel, Octasic, PMC-Sierra, Space Codesign, Technocap, Thales, Tundra, and Wavelite. He is a Fellow of the Canadian Academy of Engineering. He is the co-director of the Regroupement Stratégique en Microélectronique du Québec (RESMIQ) and a member of the Ordre des Ingénieurs du Québec (OIQ). In 2001, he was awarded a Tier 1 Canada Research Chair (www.chairs.gc.ca) on the design and architecture of advanced microelectronic systems, which he held until June 2015. He also received a Synergy Award from Canada's Natural Sciences and Engineering Research Council in 2006. Since June 2019, he has been the NSERCKaloom-Intel-Noviflow (KIN) Chair professor.

AHMED LAKHSSASSI (Senior Member, IEEE) received the B.Eng. and M.Sc.A. degrees in electrical engineering from Université du Québec á Trois-Riviéres (UQTR), Québec, Canada, in 1988 and 1990, respectively, and the Ph.D. degree in energy and material sciences from INRS-Energie et Matériaux (Institut National de la Recherche Scientifique), Québec, in 1995. In the same year also, he became a Professor of electro-thermo-mechanical aspects with NSERC-Hydro-Quebec Industrial Research Chair, Electrical Engineering Department, UQTR, where for several years, he conducted electro-thermal research projects. Since 1998, he has been with Université du Québec en Outaouais (UQO), where he is currently a Titular Professor and responsible with the LIMA Laboratory (Advanced Microsystem Engineering Laboratory) developing IP core and embedded algorithms for microsystems thermo-mechanical sensors dedicated for thermal peak detection. His research interests include bio-heat thermal modeling, such as heat diffusion in biological tissues, metabolic heat generation and external interactions, heat transfer mechanism in biological tissues for thermal therapeutic practices, including dedicated bio-implantable puce design for cancer thermal dose control. Furthermore, his research interests include machine learning to recognize the type of pain and to quantify the amount of pain to tracks any potential injury using neural networks and thermal image processing. Also, his research interest is in design of fully automated tool for porting analog and mixed signal circuits within different technology nodes. He is the Ordre des Ingénieurs du Québec (OIQ), Canada, NanoQuébec, and has more than thirty year's experience with a large expertise with applications in the fields of electro-thermo-mechanical analysis.